# Analysis of Flux Decline Behaviors in Filtration of Very Dilute Suspensions

**Eiji Iritani, Nobuyuki Katagiri, and Yuuki Sugiyama**
Dept. of Chemical Engineering, Nagoya University, Furo-cho, Chikusa-ku, Nagoya 464-8603, Japan

**Koichi Yagishita**
Sanshin Mfg. Co. Ltd., Haguro, Inuyama 484-0894, Japan

*DOI 10.1002/aic.11271*
*Published online August 1, 2007 in Wiley InterScience (www.interscience.wiley.com).*

*The gradual decrease in the filtration flux rate with time, which occurred due to the capture of solid particles and/or organic substances onto the surfaces of pores in a thin filter medium, was measured in constant-pressure filtration of both pool water and pond water. A new theoretical background of the conventional characteristic filtration equation describing the variation of the filtration resistance of the clogged filter medium with time was afforded based on a consideration of the variation of both the porosity and the specific surface area of the filter medium caused by the capture of the solids in the Kozeny-Carman equation. The flux decline behavior depended solely on the initial filtration rate, influenced by the pore size of the filter medium and the filtration pressure. The variations of the filtration rate and the filtrate volume with the filtration time were very accurately described by the analytical solution based on the characteristic filtration equation. In the case of pond water with a relatively high turbidity compared to pool water, the transition point from depth to cake filtration was determined based on the pressure dependence of the specific filtration resistance of the filter cake, and then the flux attenuation behavior was evaluated by considering the transition from depth to cake filtration.* © 2007 American Institute of Chemical Engineers *AIChE J,* 53: 2275–2283, 2007
*Keywords: dilute suspension, pore fouling, pool water, pond water, filter medium*

## Introduction

Clarifying filtration of very dilute suspensions containing fine particles, colloids, macromolecules, and microbes conducted using a relatively thin filter medium such as a membrane and a filter paper becomes increasingly important in widely divergent fields of not only industrial processing but also purification of potable water and treatment of waste-water since it is related to the removal of contaminants in aquatic environments. In depth filtration, the particles are captured inside a porous filter medium rather than on its surface. It is well known that one of the critical problems governing the performance of these filtration processes is fouling of the filter medium, leading to severe flux decline. For a practical application of the filtration processes, it is, therefore, of great importance to understand the underlying mechanisms governing fouling of the filter medium during filtration.

Numerous models have been developed to describe the fouling of the filter medium due to pore plugging.[1–4] Among them, a series of simple laws to interpret physical mechanisms of the blockage of the pores were first proposed by Hermans and Bredée,[1] and subsequently systematized by Grace.[2] The model incorporates four different kinds of blocking filtration models: complete blocking, standard blocking, intermediate blocking, and cake modes of filtration. All the filtration laws stem from a common differential equation by

Correspondence concerning this article should be addressed to E. Iritani at iritani@nuce.nagoya-u.ac.jp.

adjusting the values of two constants. Thus, for constant-pressure filtration, we have

$$\frac{d^2\theta}{dv^2} = k\left(\frac{d\theta}{dv}\right)^n \tag{1}$$

where $\theta$ is the filtration time, $v$ is the cumulative filtrate volume per unit effective cross-sectional medium area, $n$ is the blocking index which defines the mode of filtration occurring, and $k$ is the resistance coefficient which depends on the system, the filter medium, and the conditions of filtration. The reciprocal filtration rate ($d\theta/dv$) indicates a measure of the total filtration resistance to flow $R$, related by $R = p(d\theta/dv)/\mu$, where $p$ is the applied filtration pressure, and $\mu$ is the viscosity of the filtrate. Thus Eq. 1 states that the rate of change of filtration resistance is represented by a power function of the instantaneous filtration resistance. The value of $n$ is 2, 1.5, 1, and 0, respectively, for the complete blocking, standard blocking, intermediate blocking, and cake mode of filtration. Each of these blocking filtration laws may be derived from separate physical mechanisms of the filtration process.[5] In deriving the blocking filtration laws, the filter medium is assumed to have straight-through-cylindrical pores, and the fluid flow through the pores can be described as the Hagen-Poiseuille flow. Hermia[6] derived a physical model of the intermediate blocking law that had previously been regarded as empirical, by accounting for the possibility that particles can land on top of other deposited particles. Each of these blocking filtration models has been used individually or in combinations by a number of investigators[7–17] to describe experimental observations of the flux decline caused by the blockage of the pores in the thin filter medium over the course of a filtration run. Bowen et al.[18] and Iritani et al.,[19] around the same time, indicated that the value of $n$ varied successively during filtration in dead-end microfiltration of protein solutions, employing the characteristic form of the filtration laws represented by Eq. 1. More recently, Hwang et al.[20] found a similar phenomenon in particulate microfiltration. Taking the intermediate blocking law as a starting point, Lee[21] and Iritani et al.[22] analyzed medium clogging during cake filtration.

It is, however, well known that the blocking filtration model cannot accurately describe the change of the complicated pore microstructure due to deposition in depth filtration because of the physical assumption of the straight cylindrical pore. Flux decline in depth filtration typically proceeds by deposition of particles on the internal surfaces of the pores of the filter medium. Such internal fouling may be important for cases where the feed solution has a very low concentration of foulant. For instance, Ives and Pienvichitr[23] developed a depth filtration model describing the change in pressure drop with the accumulation of deposited material in the pore interior at a constant flow rate based on alterations of the porosity and specific surface area terms in the Kozeny-Carman equation. Bolton et al. also developed a fiber-coating model based on the Kozeny-Carman equation.[24] In the model, the filter microstructure was idealized as an assembly of randomly-oriented, straight, cylindrical fibers, and it was assumed that filters plug as solids coat the surfaces of fibers, making them thicker, and reducing filter porosity and permeability.

The key objective of this current work is to examine the decline mechanisms of the long-term flux during constant pressure operation in filtration of very dilute suspensions. We attempt to develop a method for elucidating data obtained from experiments of both microfiltration of pool water and filtration of pond water under constant-pressure conditions.

## Experimental

### *Materials*

Both pool water and pond water were employed as test suspensions in this research. Pool water was obtained from an indoor heated swimming pool (Tarui-cho, Fuwa-gun, Gifu). In the pool, pool water is circulated through diatomite filtration. The turbidity measured by a turbidimeter (2100AN, HACH) was 0.19 NTU. Also, the concentration of the suspended solids measured by a multipurpose rapid water quality analyzer (DR/2500 Spectrophotometer, HACH) was 0.28 mg/l. In contrast, pond water was collected from Nekogahora pond (Chikusa-ku, Nagoya). Both the turbidity and the concentration of suspended solids were 19.4 NTU and 18.0 mg/l. Thus, pond water is much more contaminated compared with pool water. Both suspensions were stored at a constant temperature of 5°C in the refrigerator until they are used.

In microfiltration of pool water, the filter medium used was a microfiltration membrane, made of a mixed cellulose ester, with a nominal pore size of 0.1, 0.2, and 0.45 $\mu$m, respectively, procured from Advantec Toyo Corp. In filtration of pond water, the filter medium used was a filter paper, 5A, 5B, and 5C, with a particle retention of 7, 4, and 1 $\mu$m, respectively, supplied by Advantec Toyo Corp.

### *Experimental apparatus and technique*

A schematic diagram of the experimental apparatus for filtration is shown in Figure 1. All experiments were performed in a dead-end filtration cell (KS-25, Advantec Toyo Corp.) with a filtration area of 3.63 cm$^2$. The filtration cell consisted essentially of a stainless-steel cylindrical vessel, equipped with

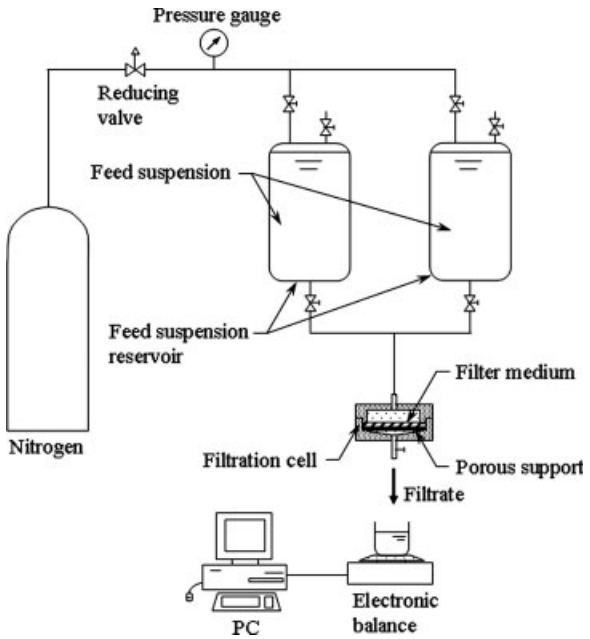


**Figure 1. Schematic diagram of experimental apparatus.**

a porous support on which the filter medium was placed. Dead-end filtration experiments were performed under conditions of constant pressure ranging from 49 to 196 kPa controlled by a reducing valve by applying compressed nitrogen gas after the test suspension was introduced into both the filtration cell and acrylic feed suspension reservoirs. To continue filtration, the feed suspension was supplied to one reservoir when it became almost empty.

The filtrate was collected in a reservoir placed on an electric balance connected to a personal computer to collect and record filtrate mass versus filtration time data. The weights were converted to volumes using filtrate density correlations. The instantaneous filtration rate was obtained by numerical differentiation of the filtrate volume versus filtration time data. The turbidity of the filtrate collected was also measured.

## Model Development

### *Depth filtration equation*

When particles are substantially smaller than the sizes of pores in a filter medium such as a membrane and a filter paper, deposition occurs by being trapped within the internal structure of the filter medium, resulting in a dramatic decline of the filtration rate. In other words, as particles are deposited, the pores become constricted and the permeability of the filter medium is reduced. A simple approach is to consider the flow of the porous medium to be represented by the Kozeny-Carman equation. Thus the filtration rate ($dv/d\theta$) in constant-pressure depth filtration is described by

$$\frac{dv}{d\theta} = \frac{\varepsilon^3}{k_0 S^2 (1-\varepsilon)^2} \cdot \frac{p}{L} \tag{2}$$

where $\varepsilon_0$ is the porosity of the filter medium, $S$ is the specific surface area of the filter medium, $L$ is the thickness of the filter medium, and $k_0$ is the Kozeny constant, which has an approximate value of 5.0.

The initial porosity $\varepsilon$ of the clean filter medium is given by

$$\varepsilon_0 = \frac{\pi}{4} N_p {D_0}^2 \tag{3}$$

where $N_p$ is the number of pores per unit cross-sectional medium area, and $D_0$ is the original representative diameter of pores on a flow cross-sectional area basis. The voids decrease as particle accumulation within the pores increases. For simplicity, in this investigation it is assumed that the particle accumulation is proportional to the filtrate volume. Therefore, the porosity $\varepsilon$ of pores coated by the deposit can be written as

$$\varepsilon = \frac{\pi}{4} N_p D^2 = \frac{\pi}{4} N_p {D_0}^2 - \frac{\pi}{4} K {D_0}^2 v \tag{4}$$

where $D$ is the representative diameter of pores on a flow cross-sectional area basis, and $K$ is an empirical constant. Combining Eqs. 3 and 4 yields

$$\varepsilon = \left(1 - \frac{Kv}{N_p}\right)\varepsilon_0 \tag{5}$$

which is equivalent to

$$\frac{D}{D_0} = \left(1 - \frac{Kv}{N_p}\right)^{1/2} \tag{6}$$

The initial specific surface area $S_0$ is described as

$$S_0 = \frac{\pi N_p D_{s0}}{1-\varepsilon_0} \tag{7}$$

where $D_{s0}$ is the original representative diameter of pores on a wetted perimeter basis. The coated specific surface area $S$ is given by

$$S = \frac{\pi N_p D_s}{1-\varepsilon} \tag{8}$$

where $D_s$ is the representative diameter of pores on a wetted perimeter basis. Depending on the mode of deposit morphology, the relation between the diameter $D_s$ on a wetted perimeter basis and the diameter $D$ on a flow cross-sectional area basis is assumed to be represented by

$$\frac{D_s}{D_{s0}} = \left(\frac{D}{D_0}\right)^{\beta} \tag{9}$$

where $\beta$ is a constant.

Combining Eqs. 7 and 8 with the aid of Eqs. 6 and 9 yields

$$S^2(1-\varepsilon)^2 = \left(1 - \frac{Kv}{N_p}\right)^{\beta} {S_0}^2 (1-\varepsilon_0)^2 \tag{10}$$

Substituting Eqs. 5 and 10 into Eq. 2, the filtration rate ($dv/d\theta$) as a function of filtrate volume $v$ can be shown to have the relation

$$\frac{dv}{d\theta} = \left(1 - \frac{Kv}{N_p}\right)^{3-\beta} \left(\frac{dv}{d\theta}\right)_0 \tag{11}$$

where $(dv/d\theta)_0$ is the initial filtration rate defined by

$$\left(\frac{dv}{d\theta}\right)_0 = \frac{{\varepsilon_0}^3}{k_0 {S_0}^2 (1-\varepsilon_0)^2} \cdot \frac{p}{L} \tag{12}$$

Equation 11 describes the variation of the filtration rate ($dv/d\theta$) with the filtrate volume $v$. By putting $\beta$ as unity, Eq. 11 reduces to the standard blocking law in which particles uniformly accumulate on the walls of straight cylindrical pores. Equation 11 can be rearranged to give

$$\frac{d\theta}{dv} = (1+Nv)^M \left(\frac{d\theta}{dv}\right)_0 \tag{13}$$

where $N = -K/N_p$, and $M = \beta - 3$. To obtain an analytical expression for the filtrate volume $v$ as a function of filtration time $\theta$. Eq. 13 can be integrated between the limits ($\theta = 0$, $v = 0$) and ($\theta = \theta$, $v = v$) as

$$v = \frac{1}{N}\left[\left\{N(M+1)\left(\frac{dv}{d\theta}\right)_0 \theta + 1\right\}^{\frac{1}{M+1}} - 1\right] \tag{14}$$

Equation 14 is not satisfactory for the special case of $M = -1$. In this case, Eq. 13 integrates to become

$$v = \frac{1}{N}\left\{\exp\left(N\left(\frac{dv}{d\theta}\right)_0 \theta\right) - 1\right\} \tag{15}$$

Differentiating Eq. 13 with respect to the filtrate volume $v$ would produce Eq. 1, where $k = MN(d\theta/dv)_0^{1/M} = (3 -$

$\beta)K(d\theta/dv)_0^{1/(\beta-3)}/N_p$, and $n = (M - 1)/M = (\beta - 4)/(\beta - 3)$. The derived equation is equivalent to the characteristic form of the filtration laws proposed by Hermans and Bredée.[1] However, according to their model, Eq. 1 was applicable just for some specified $n$-values: 2, 1.5, 1, and 0. Moreover, each $n$-value was derived from the quite different fouling mechanism. According to our model, Eq. 1 is applicable to an arbitrary $n$-value, and stems from a single fouling mechanism in which both the porosity and the specific surface area vary along with the deposition of particles on the internal surfaces of the pores of the filter medium. In this sense the derivation of Eq. 1 presented in this article is more universal, and the developed model widely extends the range of application of Eq. 1.

### *Transition from depth to cake filtration*

When the limiting capacity of pore has been reached due to deposition of particles over a long time, the build up of a filter cake on the medium surface occurs, and particles accumulate on the surface of the permeable cake. The increasing thickness of this cake adds resistance to the flow.[25,26] For the case where filtration is cake-controlled, the value of $n$ rapidly drops to zero,[20] and then Eq. 1 reduces to

$$\frac{d^2\theta}{dv^2} = k_c \tag{16}$$

where $k_c$ is the specific filtration resistance on a unit filtrate volume basis of constant-pressure cake filtration and represents the value of $d^2\theta/dv^2$ at the critical point making the transition from depth to cake filtration. Applying the classical cake filtration model,[27] the value of $k_c$ can be determined from

$$k_c = \frac{\mu\rho s\alpha_{av}}{(1 - ms)p} \tag{17}$$

where $\rho$ is the density of the filtrate, $s$ is the mass fraction of solids in suspension, $m$ is the ratio of the mass of wet to mass of dry cake, and $\alpha_{av}$ is the average specific filtration resistance and can be empirically related to the filtration pressure $p$ by a power function as[28]

$$\alpha_{av} = \alpha_0 p^{n_c} \tag{18}$$

where $\alpha_0$ and $n_c$ are the empirical fitting parameters. The exponent $n_c$ is an indication of the compressibility of the filter cake formed on the filter medium. The larger the value of $n_c$, the higher the compressibility of the cake. The expression for $\alpha_{av}$, Eq. 18, can now be substituted into Eq. 17 to obtain

$$k_c = \frac{\mu\rho s\alpha_0}{1 - ms} p^{n_c - 1} = K_c p^{n_c - 1} \tag{19}$$

where $K_c$ is a constant. Consequently, it is concluded that the transition point from depth to cake filtration can be determined based on the pressure dependence of the specific filtration resistance of the filter cake.

## Results and Discussion

### *Flux decline history*

Experimental data of microfiltration of pool water conducted using the 0.2-$\mu$m membrane under different applied pressures are plotted in Figure 2 as the form of the reciprocal filtration rate against the filtrate volume $v$ collected per unit effective membrane area. The average turbidity of the filtrate was 0.04 NTU, and thus 79% of turbidity was rejected by the microfiltration membrane. The initial filtration rate for various filtration pressures ranged from $1.64 \times 10^{-3}$ to $5.56 \times 10^{-3}$ m/s. In each case the filtration resistance increases gradually in the early stages of filtration, but undergoes a significant increase when the filtrate volume $v$ becomes large. As a consequence, the filtrate volume $v$ ceases to increase even though filtration continues. To continue the filtration operation thereafter, the cleaning operation such as backwashing and chemical cleaning etc. must become part of the process. As the filtration pressure $p$ increases, a rapid rise in the filtration resistance is seen in larger filtrate volume. In other words, the membrane fouling proceeds gradually as the filtration pressure $p$ increases. This is presumably because the lower flow rate at the lower pressure is more susceptible to rapid membrane fouling. Figure 3 shows the behavior of the filtration resistance with pore sizes $d_m$ of the membranes varying from 0.1 to 0.45 $\mu$m during the constant pressure, $p$ = 98 kPa. The initial filtration rate ranged from $4.4 \times 10^{-4}$ to $7.14 \times 10^{-3}$ m/s, depending on the pore size of the membrane. Obviously, the increase in the pore size retards a rapid increase in the filtration resistance.

In Figures 4 and 5, the reciprocal filtration rate ($d\theta/dv$) obtained in filtration of pond water is plotted against the filtrate volume $v$ for the various values of the filtration pressure $p$ and the particle retention size $d_r$ of the filter paper, respectively. The average turbidity of the filtrate was 1.5 NTU, and thus 92% of the turbidity in the pond water was removed by filtration. The results for pond water are qualitatively similar to those for pool water shown in Figures 2 and 3. However, it should be noted that the transition from gradual to the rapid increase in the filtration resistance becomes sharp in comparison to the results of pool water and that the plots after the transition seem quite linear.

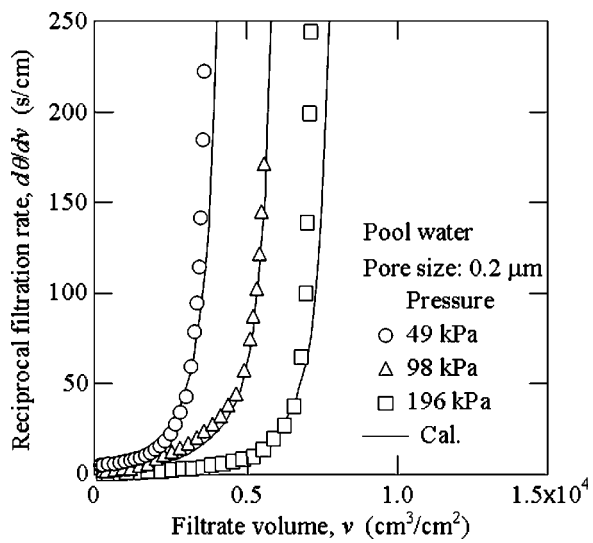


**Figure 2. Effect of filtration pressure $p$ on relation between reciprocal filtration rate ($d\theta/dv$) and filtrate volume $v$ per unit membrane area for pool water.**

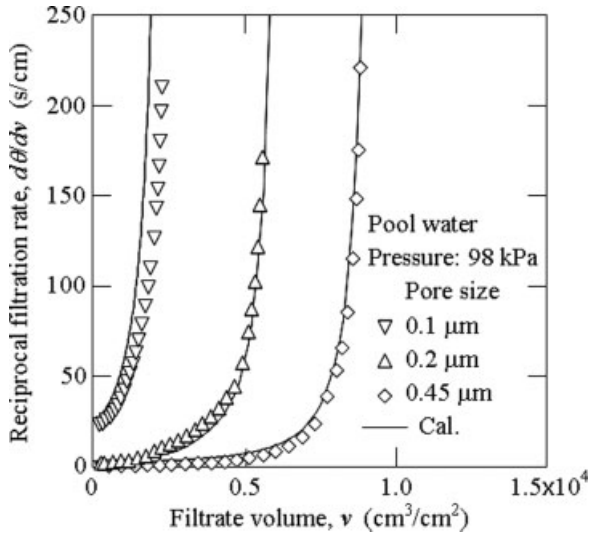


**Figure 3. Effect of pore size $d_m$ of membrane on relation between reciprocal filtration rate ($d\theta/dv$) and filtrate volume $v$ per unit membrane area for pool water.**

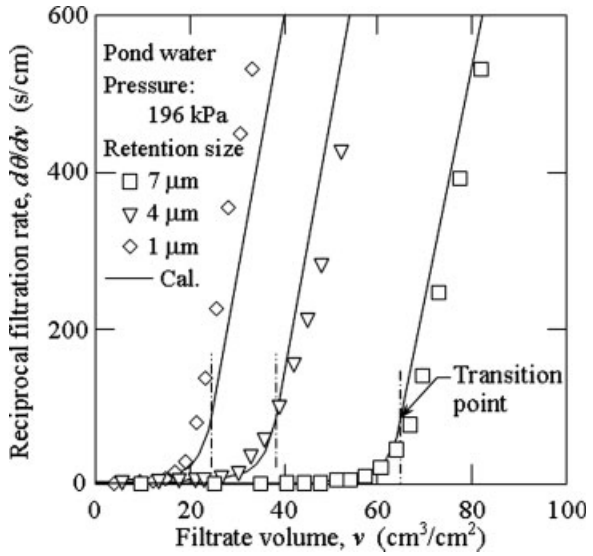


**Figure 5. Effect of particle retention size $d_r$ of filter paper on relation between reciprocal filtration rate ($d\theta/dv$) and filtrate volume $v$ per unit medium area for pond water.**

### *Characteristic form of filtration*

On the basis of the data shown in Figures 2–5, we can obtain the relationship between the first and second derivatives of the filtration time $\theta$ versus the filtrate volume $v$ per unit filter medium area. To provide a clear indication of the dominant fouling mechanism, the logarithmic plots of $d^2\theta/dv^2$ as a function of $d\theta/dv$ are shown in Figure 6 as the characteristic filtration curves. In the calculation, the second derivative ($d^2\theta/dv^2$) can be evaluated by numerical differentiation of the first derivative ($d\theta/dv$). Therefore, there is some scatter in the results due to the stepwise differentiation of the raw data. What is interesting to note here is that for pool water the data collapse to nearly a straight line in the ranges investigated in accordance with Eq. 1, irrespective of the filtration pressure and the pore size of the membrane when plotted in this manner. As the filtration proceeds and $d\theta/dv$ increases, the derivative ($d^2\theta/dv^2$) increases with $d\theta/dv$ linearly. The best fit for our experimental data gives an $n$-value (slope of logarithmic expression of Eq. 1) of about 1.46, which is slightly less than the value of 1.5 for the standard blocking law, leading to a $\beta$-value of 0.826.

In contrast to the data for pool water, the plots for pond water are approximately divided into two distinct regions. In

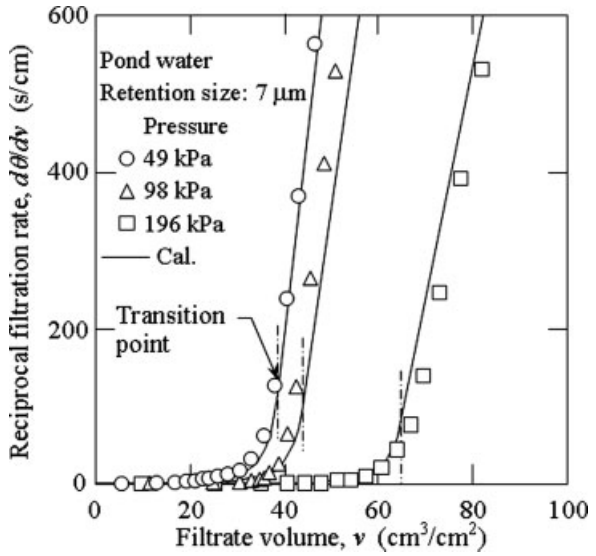


**Figure 4. Effect of filtration pressure $p$ on relation between reciprocal filtration rate ($d\theta/dv$) and filtrate volume $v$ per unit medium area for pond water.**

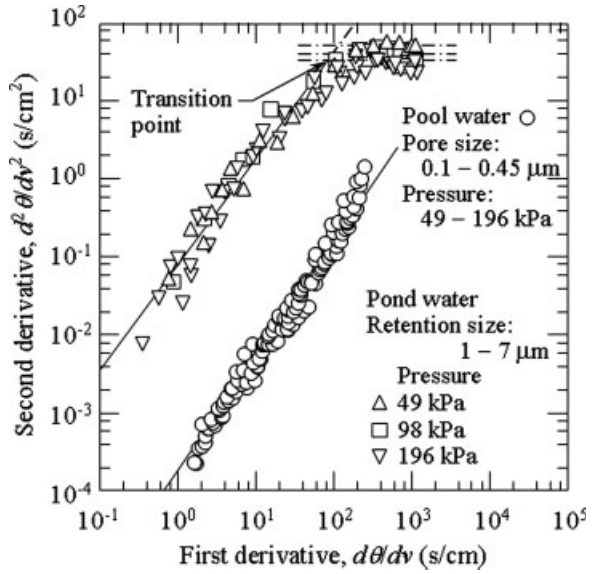


**Figure 6. Logarithmic plots of $d^2\theta/dv^2$ versus $d\theta/dv$ for both pool water and pond water.**

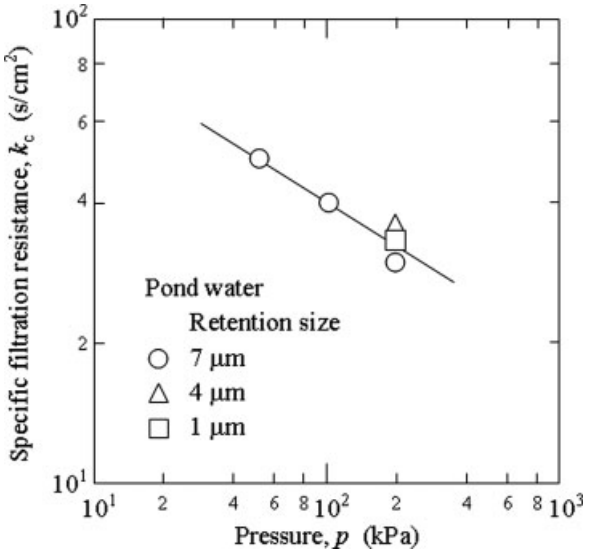


**Figure 7. Dependence of $k_c$ in Eq. 16 on filtration pressure $p$.**

the first stage of filtration (i.e., small $d\theta/dv$), plots show a unique linear relationship, irrespective of the filtration pressure and the particle retention size of the filter paper. This is similar to the results for pool water. However, the corresponding value of $d^2\theta/dv^2$ at an arbitrary value of $d\theta/dv$ becomes larger in the case of pond water with a relatively high turbidity compared to pool water. The value of $n$ determined from the slope of a straight line is about 1.35, a value between the standard blocking law ($n = 1.5$) and the intermediate blocking law ($n = 1$), leading to a $\beta$-value of 0.143. As filtration proceeds, the reciprocal filtration rates ($d\theta/dv$) increases and thus its derivative ($d^2\theta/dv^2$) increases. Once the value of $d^2\theta/dv^2$ reaches the limiting value, which depends on the filtration pressure, the second stage begins and the value of $d^2\theta/dv^2$ remains constant, as given by Eq. 16. This confirms that filtration is cake layer controlling.

The effect of the filtration pressures on $k_c$ in Eq. 16 is illustrated in logarithm scales, as shown in Figure 7. The plots appeared to be linear agreeing with Eq. 19. An increase in the filtration pressure leads to a lower $k_c$. This implies that the value of $\alpha_{av}$ increases with increasing filtration pressure because of cake compaction, with the packing density of the cake increasing with increasing pressure. The value of $n_c$ determined from the slope of the straight line was about 0.69, indicating the relatively high compressibility of the filter cake.

### *Evaluation of flux decline behaviors*

In the case of pool water, the flux decline behaviors are evaluated based on Eq. 1, which is the characteristic form of depth filtration. As the logarithmic plots of $d^2\theta/dv^2$ as a function of $d\theta/dv$ were approximated by a straight line, it is necessary to emphasize that the variations of the filtration rate and the filtrate volume during the depth filtration period depend solely on the initial filtration rate for a given suspension. The solid curves in Figures 2 and 3 represent the model calculations given by Eq. 13, using the initial value of the reciprocal filtration rate, $(d\theta/dv)_0$, and the values of $M$ and $N$. The values of $M$ and $N$ were calculated from the values of $n$ and $k$ determined from the equation form of a straight line in Figure 6. In each case the calculations are in relatively good agreement with the experimental data.

In Figure 8, the experimental data shown in Figures 2 and 3 are replotted in the form of the filtrate volume $v$ per unit membrane area versus the filtration time $\theta$. As the filtration pressure $p$ and the pore size $d_m$ of the membrane increase, the value of the filtrate volume $v$ obtained per unit filtration time $\theta$ increases. The calculations obtained using Eq. 14 are also shown in the figure and compared favorably with the experimental data.

In the case of pond water, the flux decline behaviors are evaluated based on Eq. 1, which is the characteristic form of depth filtration, and Eqs. 16 and 19, which are the filtration rate equation for cake filtration. The solid curves in Figures 4 and 5 are the calculated values. In the depth filtration period, the calculations are obtained based on Eq. 13, using the initial value of the reciprocal filtration rate, $(d\theta/dv)_0$, and the values of $M$ and $N$. Subsequently, the value of $d^2\theta/dv^2$ at the transition point between depth and cake filtration can be determined from Eq. 16 employing the value of $k_c$ obtained from Eq. 19 using the values of $K_c$ and $n_c$. The values of $K_c$ and $n_c$ were determined from the equation form of a straight line in Figure 7. The value of the reciprocal filtration rate $(d\theta/dv)$ at the transition point can be obtained by substituting the value of $d^2\theta/dv^2$ thus obtained into Eq. 1. Since $n = 0$ and $k = k_c$ in cake filtration, by replacing $v$ and $(d\theta/dv)_0$ by $(v - v_t)$ and $(d\theta/dv)_t$, respectively, Eq. 13 reduces to

$$\frac{d\theta}{dv} = k_c(v - v_t) + \left(\frac{d\theta}{dv}\right)_t \tag{20}$$

where the subscript $t$ is used to denote the value at the transition point. The above equation is in accordance with the

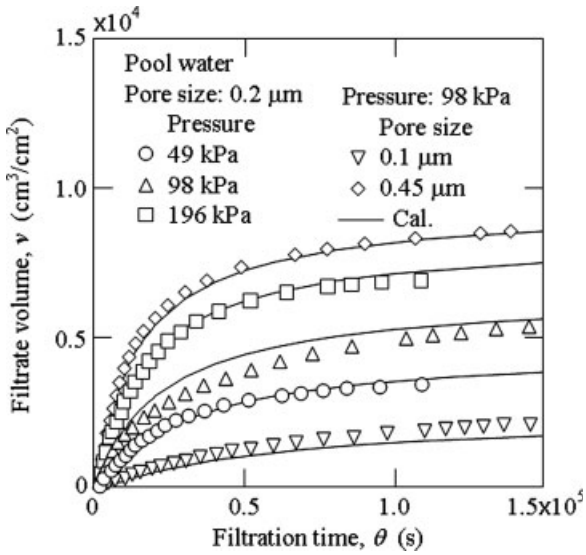


**Figure 8. Relation between filtrate volume $v$ per unit membrane area and filtration time $\theta$ for pool water.**

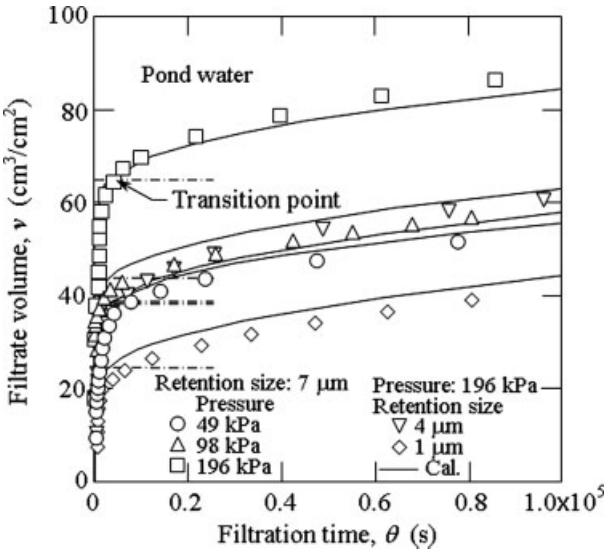


**Figure 9. Relation between filtrate volume $v$ per unit medium area and filtration time $\theta$ for pond water.**

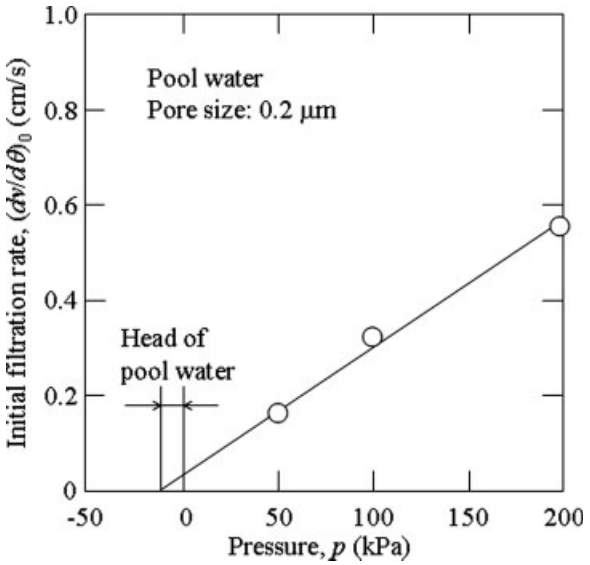


**Figure 10. Relation between initial filtration rate $(dv/d\theta)_0$ and the filtration pressure $p$ for pool water.**

conventional cake filtration equation.[8] Thus, the relation between $d\theta/dv$ and $v$ at the late stage of filtration after the transition point is given by Eq. 20. The calculations are in fairy good agreement with all experimental data in both the depth and cake filtration periods. A significant part of the resistance was due to cake filtration rather than depth filtration.

Figure 9 represents the experimental data of $v$ versus $\theta$ for the results of pond water shown in Figures 4 and 5. The experimental data are compared with the calculations, good agreement being observed throughout a range of filtration. The calculations during the cake filtration period are obtained by substituting both $n = 0$ and $k = k_c$ into Eq. 14 and by replacing $v$, $\theta$, and $(dv/d\theta)_0$ by $(v - v_t)$, $(\theta - \theta_t)$, and $(dv/d\theta)_t$, respectively, yielding

$$k_c\left(\frac{dv}{d\theta}\right)_t (v - v_t)^2 + 2(v - v_t) = 2\left(\frac{dv}{d\theta}\right)_t (\theta - \theta_t) \qquad (21)$$

where $\theta_t$ is the filtration time at the transition point.

### *Simulation based on characteristic form of filtration*

It is quite important to note that behaviors of flux decline depend on the initial reciprocal filtration rate $(d\theta/dv)_0$ (i.e., the initial filtration rate $(dv/d\theta)_0$) alone for a given suspension to be filtered. Consistent with Eq. 12, the initial filtration rate $(dv/d\theta)_0$ increases approximately linearly with increasing applied filtration pressure $p$ in the regime of laminar flow[29] as typically shown in Figure 10 for pool water since the membrane is incompressible at the pressures used in these experiments. Therefore, the effect of the filtration pressure $p$ on the flux decline behavior is reflected by changing the value of the initial reciprocal filtration rate $(d\theta/dv)_0$. The intercept of the abscissa corresponds to the average head of pool water contained in the feed suspension reservoir. Figure 11 shows the simulations of $d\theta/dv$ versus $v$ in microfiltration of pool water for the various values of the filtration pressure $p$. The model follows the observed trend shown in Figure 2. It is obvious that the filtrate volume $v$, where reciprocal filtration rate $d\theta/dv$ increases sharply, increases with increasing filtration pressure $p$. In pool water the values of $n$ and $k$ in Eq. 1 are 1.46 and $1.91 \times 10^{-4}$ $s^{1-n}/cm^{2-n}$, respectively. The effects of changing either $n$ or $k$ on the flux decline behaviors are examined in more detail in Figures 12 and 13, respectively. Of interest is that the curvature becomes smaller with decreasing $n$. In cases that $n = 0$, a linear relationship is obtained in accordance with the relation in cake filtration expressed as Eq. 20. The change in $k$ affects the rising behaviors of the reciprocal filtration rate as in the case of the filtration pressure.

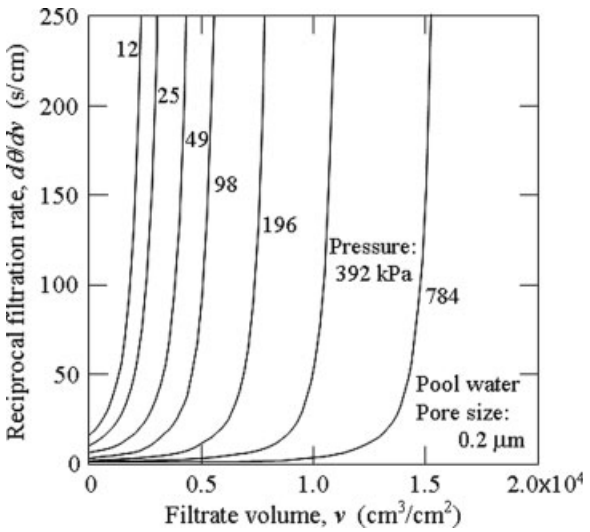


**Figure 11. Simulation results of relation between reciprocal filtration rate $(d\theta/dv)$ and filtrate volume $v$ per unit membrane area at various filtration pressures for pool water.**

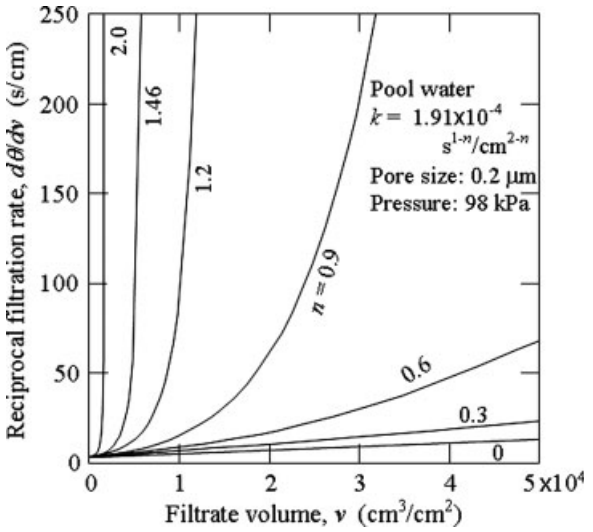


**Figure 12. Simulation results of relation between reciprocal filtration rate ($d\theta/dv$) and filtrate volume $v$ per unit membrane area at various values of $n$ for pool water.**

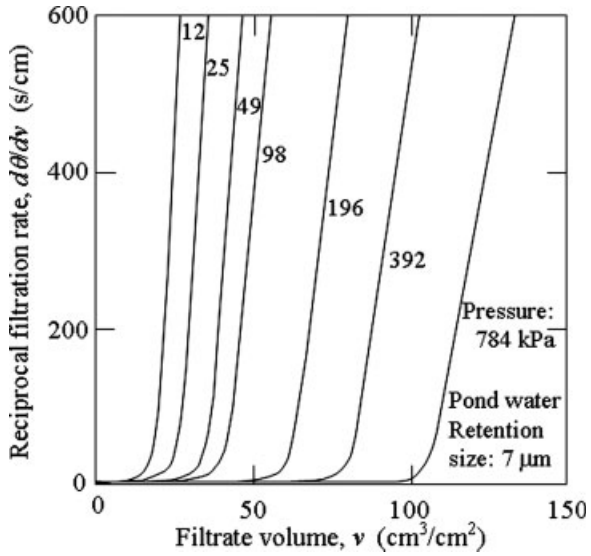


**Figure 14. Simulation results of relation between reciprocal filtration rate ($d\theta/dv$) and filtrate volume $v$ per unit medium area at various filtration pressures for pond water.**

In Figure 14, the simulation results of $d\theta/dv$ versus $v$ in filtration of pond water are illustrated for the various values of the filtration pressure $p$. In this case the fouling of the filter medium starts with depth filtration and then is followed by continuous cake formation. Thus the flux decline trend becomes more complex. It must be stressed, once again, that the transition point from depth to cake filtration can be determined based on the pressure dependence of the specific filtration resistance of the filter cake. It is evident that the filtrate volume $v$ at the transition point, where the filtration mechanism changes from depth to cake filtration, tends to increase with the increase in the filtration pressure $p$. The trends of the calculations are similar to those shown in Figure 11, but the results of pond water show a linear relationship in the period of cake filtration, whereas there is a definite curvature for the results of pool water. From a practical point of view, it is quite important to know when backwashing or replacement of the fouled filter medium should be conducted. Evaluating the filtrate volume or filtration time at which the increase in the filtration resistance becomes more pronounced makes it easy to determine the time at which backwashing of the filter medium should be conducted.

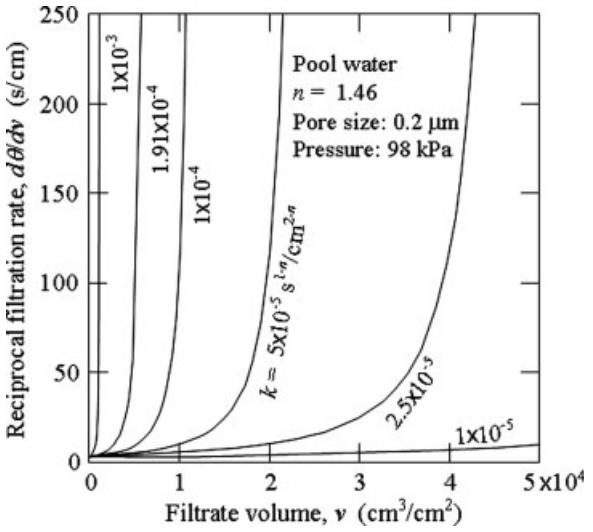


**Figure 13. Simulation results of relation between reciprocal filtration rate ($d\theta/dv$) and filtrate volume $v$ per unit membrane area at various values of $k$ for pool water.**

## Conclusions

The flux decline behaviors in constant-pressure filtration of very dilute suspensions varying filtration pressures and pore sizes of the filter medium were examined by employing pool water and pond water. The filtration resistance increases gradually in the early stages of filtration, but exhibits a dramatic increase when the filtrate volume becomes large. As the filtration pressure and the pore size of the filter medium increases, a rapid rise in the filtration resistance is seen in larger filtrate volume. In this regard, the results for pool water and pond water are superficially similar to each other. However, in the case of pond water with a relatively high turbidity, the filtration mechanism shifted from depth to cake filtration.

A new theoretical background of the conventional characteristic filtration equation describing the rate of change in the filtration resistance of the clogged filter medium was afforded by accounting for the variation of both the porosity and the specific surface area of the filter medium caused by the capture of the solids explicitly in the Kozeny-Carman equation. The variations of the filtration rate and the filtrate volume with the filtration time of pool water were well evaluated based on the characteristic filtration equation. As a result, it was demonstrated that the flux decline behavior depends solely on the initial filtration rate under a given suspension. In the case of pond

water with a relatively high turbidity, the transition point from depth to cake filtration was determined with the aid of the specific filtration resistance of cake filtration under the constant-pressure conditions, and then the flux decline behavior was well evaluated based on the characteristic filtration equation.

## Acknowledgments

This work has been supported in part by a Grant-in-Aid for Scientific Research from The Ministry of Education, Culture, Sports, Science and Technology, Japan. The authors wish to acknowledge with sincere gratitude the financial support leading to the publication of this article. The authors also thank K. Hayashi and M. Kurano for their assistances in carrying out the experiments, and K. Kondo of Sanshin Mfg. Co. Ltd. for kindly sampling the pool water.

## Notation

$D$ = representative diameter of pores of flow cross-sectional area basis, m
$D_s$ = representative diameter of pores of wetted perimeter basis, m
$d_m$ = nominal pore size of membrane, m
$d_r$ = particle retention size of filter medium, m
$K$ = constant in Eq. 4, $m^{-3}$
$K_c$ = constant in Eq. 19, $kg^{1-n_c}\ m^{n_c-3}\ s^{2n_c-1}$
$k$ = constant in Eq. 1, $m^{n-2}\ s^{1-n}$
$k_0$ = Kozeny constant
$k_c$ = specific filtration resistance of unit filtrate volume basis of constant-pressure filtration in Eq. 16, $s/m^2$
$L$ = thickness of filter medium, m
$M$ = constant in Eq. 13
$m$ = ratio of mass of wet to mass of dry cake
$N$ = constant in Eq. 13, $m^{-1}$
$N_p$ = number of pores per unit cross-sectional medium area, $m^{-2}$
$n$ = constant in Eq. 1
$n_c$ = constant in Eq. 18
$p$ = applied filtration pressure, Pa
$R$ = filtration resistance, $m^{-1}$
$S$ = specific surface area of filter medium, $m^{-1}$
$s$ = mass fraction of solids in slurry
$v$ = cumulative filtrate volume per unit effective medium area, $m^3/m^2$

### *Greek letters*

$\alpha_0$ = constant in Eq. 18, $kg^{-1-n_c}\ m^{1+n_c}\ s^{2n_c}$
$\alpha_{av}$ = average specific filtration resistance, m/kg
$\beta$ = constant in Eq. 9
$\varepsilon$ = porosity of filter medium
$\theta$ = filtration time, s
$\mu$ = viscosity of filtrate, Pa s
$\rho$ = density of filtrate, $kg/m^3$

### *Subscripts*

0 = initial value
t = value at transition

## Literature Cited

1. Hermans PH, Bredée HL. Principles of the mathematical treatment of constant-pressure filtration. *J Soc Chem Ind*. 1936;55T:1–4.
2. Grace HP. Structure and performance of filter media. II. Performance of filter media in liquid service. *AIChE J*. 1956;2:316–336.
3. Heertjes PM. Studies in filtration: blocking filtration. *Chem Eng Sci*. 1957;6:190–203.
4. Fan LT, Hwang SH, Nassar R, Chou ST. An experimental study of deep-bed filtration: stochastic analysis. *Powder Technol*. 1985;44:1–11.
5. Granger J, Dodds J, Leclerc D. Filtration of low concentrations of latex particles on membrane filters. *Filtr Sep*. 1985;22:58–60.
6. Hermia J. Constant pressure blocking filtration laws—application to power-law non-Newtonian fluids. *Trans IChemE*. 1982;60:183–187.
7. Iritani E, Sumi H, Murase T. Analysis of filtration rate in clarification filtration of power-law non-Newtonian fluids-solids mixtures under constant pressure by stochastic model. *J Chem Eng Jpn*. 1991;24:581–586.
8. White DA. The interpretation of the SDI for water solids content using the filtration equation. *Trans IChemE Part B: Process Saf Environ Prot*. 1996;74:137–140.
9. Blanpain-Avet P, Filaudeau L, Lalande M. Investigation of mechanisms governing membrane fouling and protein rejection in the sterile microfiltration of beer with an organic membrane. *Trans IChemE Part C: Food Bioprod Process*. 1999;77:75–89.
10. Ho CC, Zydney AL. A combined pore blockage and cake filtration model for protein fouling during microfiltration. *J Colloid Interface Sci*. 2000;232:389–399.
11. Boerlage SFE, Kennedy MD, Dickson MR, El-Hodali DEY, Schippers JC. The modified fouling index using ultrafiltration membranes (MFI-UF): characterization, filtration mechanisms and proposed reference membrane. *J Membr Sci*. 2002;197:1–21.
12. De Bruijn JPF, Salazar FN, Bórquez R. Membrane blocking in ultrafiltration: a new approach to fouling. *Trans IChemE Part C: Food Bioprod Process*. 2005;83:211–219.
13. Purkait MK, Bhattacharya PK, De S. Membrane filtration of leather plant effluent: flux decline mechanism. *J Membr Sci*. 2005;258:85–96.
14. Bolton G, LaCasse D, Kuriyel R. Combined models of membrane fouling: development and application to microfiltration and ultrafiltration of biological fluids. *J Membr Sci*. 2006;277:75–84.
15. Duclos-Orsello C, Li W, Ho CC. A three mechanism model to describe fouling of microfiltration membranes. *J Membr Sci*. 2006;280:856–866.
16. Gironès M, Lammertink RGH, Wessling M. Protein aggregate deposition and fouling reduction strategies with high-flux silicon nitride microsieves. *J Membr Sci*. 2006;273:68–76.
17. Mourouzidis-Mourouzis SA, Karabelas AJ. Whey protein fouling of microfiltration ceramic membranes – pressure effects. *J Membr Sci*. 2006;282:124–132.
18. Bowen WR, Calvo JI, Hernández A. Steps of membrane blocking in flux decline during protein microfiltration. *J Membr Sci*. 1995;101:153–165.
19. Iritani E, Mukai Y, Tanaka Y, Murase T. Flux decline behavior in dead-end microfiltration of protein solutions. *J Membr Sci*. 1995;103:181–191.
20. Hwang KJ, Liao CY, Tung KL. Analysis of particle fouling during microfiltration by use of blocking models. *J Membr Sci*. 2007;287:287–293.
21. Lee DJ. Filter medium clogging during cake filtration. *AIChE J*. 1997;43:273–276.
22. Iritani E, Mukai Y, Furuta M, Kawakami T, Katagiri N. Blocking resistance of membrane during cake filtration of dilute suspensions. *AIChE J*. 2005;51:2609–2614.
23. Ives KJ, Pienvichitr V. Kinetics of the filtration of dilute suspensions. *Chem Eng Sci*. 1965;20:965–973.
24. Bolton GR, LaCasse D, Lazzara MJ, Kuriyel R. The fiber-coating model biopharmaceutical depth filtration. *AIChE J*. 2005;51:2978–2987.
25. Huang L, Morrissey MT. Fouling of membranes during microfiltration of surimi wash water: roles of pore blocking and surface cake formation. *J Membr Sci*. 1998;144:113–123.
26. Kim KJ, Chen V, Fane AG. Ultrafiltration of colloidal silver particles: flux, rejection, and fouling. *J Colloid Interface Sci*. 1993;155:347–359.
27. Ruth BF. Studies in filtration. III. Derivation of general filtration equations. *Ind Eng Chem*. 1935;27:708–723.
28. Sperry DR. Note and Correspondence: a study of the fundamental laws of filtration using plant-scale equipment. *Ind Eng Chem*. 1921;13:1163–1164.
29. Hodgson PH, Lealie GL, Schneider RP, Fane AG, Fell CJD, Marshall KC. Cake resistance and solute rejection in bacterial microfiltration: the rate of the extracellular matrix. *J Membrane Sci*. 1993;79:35–53.

*Manuscript received Apr. 20, 2007, and revision received Jun. 25, 2007.*